JGR Atmospheres

RESEARCH ARTICLE
10.1029/2018JD029852

# Drivers and Surface Signal of Interannual Variability of Boreal Stratospheric Final Warmings

**R. Thiéblemont[1,2], B. Ayarzagüena[3,4], K. Matthes[5,6], S. Bekki[7], J. Abalichin[8], and U. Langematz[8]**

[1]Laboratoire des Sciences du Climat et de l'Environnement (LSCE), CNRS, Saint-Aubin, France, [2]Now at BRGM/French Geological Survey, Orléans, France, [3]Departamento Fisica de la Tierra y Astrofisica, Universidad Complutense de Madrid (UCM), Madrid, Spain, [4]Instituto de Geociencias, CSIC-UCM, Madrid, Spain, [5]GEOMAR-Helmholtz Centre for Ocean Research, Kiel, Germany, [6]Christian-Albrechts-Universität zu Kiel (CAU), Kiel, Germany, [7]LATMOS/IPSL, Sorbonne Université, UVSQ, Université Paris-Saclay, CNRS, Paris, France, [8]Department of Earth Sciences, Institute of Meteorology, Freie Universität Berlin (FUB), Berlin, Germany

**Abstract** Springtime stratospheric final warming (SFW) variability has been suggested to be linked to the tropospheric circulation, particularly over the North Atlantic sector. These findings, however, are based on reanalysis data that cover a rather short period of time (1979 to present). The present work aims to improve the understanding of drivers, trends and surface impact of dynamical variability of boreal SFWs using chemistry-climate models. We use multidecadal integrations of the fully coupled chemistry-climate models Community Earth System Model version 1 (Whole Atmosphere Community Climate Model) and ECHAM/Modular Earth Submodel System Atmospheric Chemistry-O. Four sensitivity experiments are analyzed to assess the impact of external factors; namely, the quasi-biennial oscillation, sea surface temperature (SST) variability, and anthropogenic emissions. SFWs are classified into two types with respect to their vertical development; that is, events which occur first in the midstratosphere (10-hPa first SFWs) or first in the upper stratosphere (1-hPa first SFWs). Our results confirm previous reanalysis results regarding the differences in the time evolution of stratospheric conditions and near-surface circulation between 10 and 1-hPa first SFWs. Additionally, a tripolar SST pattern is, for the first time, identified over the North Atlantic in spring months related to the SFW variability. Our analysis of the influence of remote modulators on SFWs revealed that the occurrence of major warmings in the previous winter favors the occurrence of 10-hPa first SFWs later on. We further found that quasi-biennial oscillation and SST variability significantly affect the ratio between 1-hPa first and 10-hPa first SFWs. Finally, our results suggest that ozone recovery may impact the timing of the occurrence of 1-hPa first SFWs.

**Key Points:**
- Northern Hemisphere stratospheric final warmings variability and dynamics are studied in multidecadal chemistry-climate experiments
- Stratospheric final warmings characteristics in spring are influenced by the polar vortex variability in preceding winter
- Quasi-biennial oscillation, sea surface temperature, and ozone depleting substances influence stratospheric final warming variability

**Supporting Information:**
- Supporting Information S1

**Correspondence to:**
R. Thiéblemont,
r.thieblemont@externe.brgm.fr

**Citation:**
Thiéblemont, R., Ayarzagüena, B., Matthes, K., Bekki, S., Abalichin, J., & Langematz, U. (2019). Drivers and surface signal of interannual variability of boreal stratospheric final warmings. *Journal of Geophysical Research: Atmospheres*, *124*, 5400–5417. https://doi.org/10.1029/2018JD029852

Received 17 OCT 2018
Accepted 26 APR 2019
Accepted article online 2 MAY 2019
Published online 29 MAY 2019

**Author Contributions:**
**Data curation:** K. Matthes, S. Bekki, U. Langematz
**Formal analysis:** B. Ayarzagüena
**Funding acquisition:** S. Bekki
**Investigation:** B. Ayarzagüena
**Methodology:** B. Ayarzagüena
**Project administration:** S. Bekki
**Resources:** K. Matthes, S. Bekki, J. Abalichin, U. Langematz
**Software:** J. Abalichin
**Supervision:** K. Matthes, S. Bekki
**Writing – review & editing:** B. Ayarzagüena, K. Matthes, S. Bekki, U. Langematz



## 1. Introduction

A stratospheric final warming (SFW) consists of an irreversible breakup of the winter polar vortex, which marks the springtime transition between the winter (cyclonic) and summer (anticyclonic) dynamical regimes in the extratropical stratosphere (Black & McDaniel, 2007). SFWs occur in both hemispheres and their timing and dynamical evolution are characterized by a combination of radiative and planetary wave forcing effects. In the Northern Hemisphere, the enhanced planetary wave activity (due to larger orography and land-sea contrasts) leads to a large SFW interannual variability in its timing and vertical structure that in turn can have remarkable consequences in the stratosphere and the troposphere.

SFW onset dates vary by about 2 months and are, apart from the upward-propagating wave activity, also sensitive to the stratospheric background state (Salby & Callaghan, 2007; Waugh et al., 1999). The timing of SFWs can have consequences on polar ozone depletion and the stratospheric chemical composition in spring and summer (e.g., Manney et al., 2011). For instance, anomalously early SFWs (i.e., early vortex breakup) can lead to a rapid cessation of ozone loss as it was the case in the springs 2005 and 2016 (Manney, Santee, et al., 2006; Manney & Lawrence, 2016). Waugh and Rong (2002) also showed strong differences in the polar vortex mixing processes with midlatitude air in association with the SFW timing. More recently, Thiéblemont et al. (2011, 2013) revealed that early SFWs are more likely to feature "Frozen-In" anticyclone occurrences in spring and summer (Manney, Livesey, et al., 2006), which lead to anomalously high nitrous oxide and methane concentrations in the polar stratosphere. However, not only does the variability of SFW

timing alter the stratospheric composition and circulation, but it is also associated with tropospheric anomalies. For instance, Ayarzagüena and Serrano (2009) found significant changes in the tropospheric circulation in April, particularly over the Euro-Atlantic sector, when separating early and late SFWs in ERA-40 reanalysis.

Hardiman et al. (2011) characterized the variability of SFWs by their vertical temporal development rather than their timing: they found that in some years, SFWs occur first in the mid-stratosphere (10 hPa or ~30 km, hereafter referred to as 10-hPa first), and in others first in the upper stratosphere (1 hPa or ~50 km, hereafter referred to as 1-hPa first). They showed that years in which 10-hPa first SFWs occur are associated with a more negative North Atlantic Oscillation (NAO)-like pattern in April mean sea level pressure than years in which 1-hPa first SFWs occur. These results hence indicate that the knowledge of SFW characteristics provides additional predictability skills of springtime tropospheric climate. In this regard, it is important to identify factors that influence the variability of SFWs and to understand the associated mechanisms.

Previous findings based on reanalyses suggested that the variability of SFWs is highly dependent on stratospheric dynamical conditions in the previous winter. For instance, Waugh et al. (1999) found a very strong correlation between the activity of planetary waves entering the stratosphere two months before the SFW (diagnosed as the eddy heat flux at 100 hPa and averaged over the latitude range 45–75°N) and the polar vortex breakup date. Wei et al. (2007) related the evolution of the strength of the polar vortex and wave activity during the previous winter to the SFW timing. Hu et al. (2014) found that early spring SFWs (approximately March) are more likely to be preceded by winters unperturbed by sudden stratospheric warming (SSW) events, while late spring SFWs are mostly preceded by SSW events in midwinter. Hardiman et al. (2011) also found that the vertical profile of the SFW appears to be influenced by the strength of the polar vortex before: a weaker polar vortex tends to favor 10-hPa first SFWs. These various results hence suggest that a better understanding of the SFWs variability requires understanding the drivers of the stratospheric polar vortex dynamical variability in winter.

Numerous reanalysis and climate model studies have examined the sensitivity of the strength of the boreal stratospheric polar vortex to external and/or remote variability factors in winter such as the quasi-biennial oscillation (QBO), solar irradiance fluctuations, or oceanic variability. Holton and Tan (1980) suggested a relationship between the strength of the polar vortex and the phase of the QBO (the "Holton-Tan (HT) relationship"). Specifically, they found that the vortex is weaker on average in the easterly phase of the QBO than in the westerly phase. This relationship has afterward been supported by modeling studies using atmospheric models of various complexity (e.g., Calvo et al., 2007; Hansen et al., 2013). The influence of the QBO on the wintertime polar vortex strength has further been proposed to be modulated by the 11-year solar cycle (e.g., Camp & Tung, 2007; Matthes et al., 2013). It is also well established that the polar vortex is modulated by the El Niño–Southern Oscillation (ENSO; e.g., Garfinkel & Hartmann, 2008; Calvo et al., 2017; Domeisen et al., 2019). Relationships between sea surface temperatures (SSTs) and the winter Arctic stratosphere variability have also been found in other sectors such as the North Pacific (Hurwitz et al., 2012) and the Atlantic (Omrani et al., 2014). However, a link between these external or remote factors and SFW variability has not been established yet.

The stratospheric polar vortex is also expected to change in the future as a result of long-term anthropogenic changes in atmospheric composition, that is, increasing greenhouse gas (GHG) concentrations and stratospheric ozone layer recovery. For instance, several studies have examined possible trends in the future occurrence of midwinter SSWs (e.g., Ayarzagüena et al., 2018; Bell et al., 2010; Hansen et al., 2014; Karpechko & Manzini, 2017; Kim et al., 2017; Manzini et al., 2014; Mitchell et al., 2012; SPARC CCMVal, 2010), but no consensus has been reached yet. Nevertheless, the effects of projected climate change on SFWs have not been addressed.

Drivers of polar vortex variability and trends, and their associated mechanisms, are, by far, more documented in winter than in spring. The aim of the present study is to improve the understanding of the dynamical variability of SFWs by assessing how the QBO, variable SSTs, and anthropogenic emissions modulate their dynamical characteristics; that is, vertical profile and timing. Note also that the previous studies, which examined the dynamical features of SFWs were based on reanalysis data sets, not on climate model simulations, and so the length of observations is relatively short to derive robust conclusions. Here, we use for the first time a set of five multidecadal integrations (more than 140 years) of two fully coupled ocean-atmosphere chemistry-climate models (Community Earth System Model, CESM [Whole Atmosphere Community

**Table 1**
*Summary of CESM (WACCM) Experiments.*

| Name | Period | GHGs/ODSs | QBO | SST/sea ice |
|---|---|---|---|---|
| Natural | 1955–2099 | Fixed at 1960s level | Nudged | Interactive |
| RCP85 | 1955–2099 | **RCP8.5 scenario** | Nudged | Interactive |
| NoQBO | 1955–2099 | Fixed at 1960s level | **No** | Interactive |
| FixedSST | 1955–2099 | Fixed at 1960s level | Nudged | **Climatological** |

*Note*. Text in bold emphasizes the varying factor in the sensitivity experiment in comparison with the Natural experiment. CESM = Community Earth System Model; WACCM = Whole Atmosphere Community Climate Model; GHG = greenhouse gas; ODS = ozone depleting substance; QBO = quasi-biennial oscillation; SST = sea surface temperature.

Climate Model, WACCM] and EMAC-O) in which the external factors have been systematically switched on and off to investigate SFWs. Such long experiments allow for a large statistical sampling.

The paper is organized as follows. Section 2 describes the models, the sensitivity experiments, and the definition of the different classifications of SFWs on which the composite analysis is based. Section 3 examines the stratospheric dynamics of SFWs and the associated surface climate response simulated by the model. In section 4, we investigate the relationship between the polar vortex strength in winter and the dynamical evolution of SFWs. Section 5 assesses the influence of external factors (i.e., QBO, transient SSTs, and anthropogenic forcing) on the distribution of SFWs (according to their class) and their timing. A summary of the study is provided in section 6.

## 2. Data and Methods

### 2.1. CESM1 (WACCM)

CESM, version 1.0.2, developed at the National Center for Atmospheric Research, is a fully coupled model, which includes an interactive ocean (POP), land (CLM), sea ice (CICE), and an atmospheric component with interactive chemistry (WACCM3.5; Marsh et al., 2013). The POP ocean module has a tripolar horizontal grid of 1° × 1° and 60 depth levels. WACCM3.5 (Gent et al., 2011) uses a vertical hybrid $\sigma$-$P$ coordinate and has 66 levels and a lid height at ~140 km (~$5.1 \times 10^{-6}$ hPa). The model is integrated with a horizontal resolution of 2.5° in longitude and 1.9° in latitude. Interactive chemistry is calculated with the 3-D chemistry module based on version 3 of the Model for Ozone And Related chemical Tracers (Kinnison et al., 2007). WACCM3.5 is forced by daily spectrally resolved solar irradiance from the NRLSSI1 data set (Lean et al., 2005).

In our model version, the vertical resolution of WACCM is not high enough to internally generate a QBO. Therefore, the modeled tropical zonal winds are relaxed to observations between 22°S and 22°N using a Gaussian weighting function with a half width of 10°, which decays latitudinally from the equator (Matthes et al., 2010). The relaxation extends in the vertical from 86 to 4 hPa with a time constant of 10 days. The equatorial QBO forcing time series is determined from the climatology of 1953–2004 reconstructed from combined radiosonde (Naujokat, 1986) and rocketsonde measurements (Gray et al., 2001). The QBO is then projected into the future by developing Fourier coefficients for the QBO time series determined from the past climatology (1953–2004). More information on the QBO climatology used for the nudging procedure can be found at http://www.pa.op.dlr.de/CCMVal/Forcings/qbo_data_ccmval/u_profile_195301-200412.html website.

### 2.2. Model Experiments

To examine the influence of external variability sources on Northern Hemisphere SFWs, four CESM1 (WACCM) simulations (Hansen et al., 2014), spanning 145 years, were performed by systematically switching on and off particular variability factors as summarized in Table 1. All experiments start in January 1955 and run until December 2099. The four model experiments are forced by the NRLSSI1 (daily solar spectral irradiance data set; Lean et al., 2005) from 1955 to 2009. From 2010 to 2099, the solar forcing is prescribed by repeating twice the last four solar cycles provided in NRLSSI1. The three major volcanic eruptions observed, that is, Agung (1963), El Chichón (1982), and Mount Pinatubo (1991), are included by prescribing the volcanic forcing described in (SPARC CCMVal, 2010).

The Natural experiment simulates the natural variability of climate, that is, without including anthropogenically induced GHG and ozone concentration changes. This experiment is hence performed by keeping the concentrations of GHGs and ozone depleting substances (ODSs) constant at the 1960s level but includes all natural sources of variability such as ENSO or QBO. The RCP85, NoQBO, and FixedSST experiments are designed by modifying specific settings of the Natural experiment. In the RCP85 experiment, the observed GHG and ODS concentrations are prescribed until 2005 and the RCP8.5 scenario (Meinshausen et al., 2011) is used from 2006 onward. In the NoQBO experiment, the QBO nudging procedure is switched off, leading to weak easterlies throughout the depth of the tropical stratosphere. Finally, in the FixedSST experiment, the ocean interactive coupling is switched off and the SST is instead prescribed based on the seasonal climatology derived from the Natural experiment; the FixedSST experiment has therefore no ENSO variability. Hence, comparing the RCP85, NoQBO, and FixedSST experiments with the Natural experiment allows for quantifying the effects of anthropogenic forcing, QBO and ocean variability, respectively, on SFWs in the Northern Hemisphere.

The analyses of CESM (WACCM) simulations are compared with ERA-Interim (ERA-I) products (Dee et al., 2011), which provide meteorological reanalyses from 1979 to present (about 40 years) and cover the full troposphere/stratosphere region. CESM (WACCM) results are also compared with results of a multidecadal simulation performed with the EMAC (ECHAM/Modular Earth Submodel System Atmospheric Chemistry) chemistry-climate model (version 1.10; Jöckel et al., 2006; 140 years) run under constant 1960s levels of GHGs and ODSs, that is, comparable to the Natural CESM (WACCM) simulation. In this configuration, EMAC is fully coupled with the MPI-OM ocean module (Jungclaus et al., 2006; hereafter denoted EMAC-O; Abalichin, 2016). In the EMAC-O simulation, the QBO variability is accounted for through a nudging procedure. The EMAC-O results are shown in the supporting information.

### 2.3. Classification of SFWs and Composite Analysis

The SFW onset date is defined, at each pressure level between 50 and 1 hPa, as the time when the zonal mean zonal wind at 60°N becomes easterly without returning to westerlies until the subsequent autumn (Hardiman et al., 2011). As explained in Hardiman et al. (2011), this definition can be applied either on daily or monthly data. Although the use of daily data seems a priori more accurate, in many years the zonal mean zonal wind value at 60°N near the time of the SFW can durably fluctuate around zero before stabilizing to summer easterlies. This can make the SFW date very sensitive to small perturbations which are not representative of large scale dynamics and which may require a readjustment of the date by visual inspection or the addition of complexity in the algorithm; for example, defining zonal mean zonal wind thresholds or applying running averages on daily data (e.g., Black et al., 2006). Given the large amount of simulated years (580 in total), the number of model levels where SFW dates are defined (9 between 50 and 1 hPa) and the fact that the background zonal mean zonal wind can change between our four sensitivity experiments, the number of additional criteria to define SFW onsets may become very large and add too much subjectivity. As a consequence, instead of daily data, we used monthly data that are linearly interpolated to the day where the zonal mean zonal wind crosses the zero line at each level. Note that we used linearly interpolated monthly data only for defining the wind reversal date. All analysis performed on sub-monthly timescales (e.g., section 3) are based on daily data. Once the vertical profile of the SFW date is defined, we classify the type of SFW by comparing the dates at 10 and 1 hPa. If the SFW occurs first at 10 or 1 hPa, then it is labeled as "10-hPa first" or "1-hPa first," respectively. Note that if less than 5 days separate the SFW dates at 10 and 1 hPa, the SFW is classified as "neutral." This classification of SFWs allows the consideration of the full vertical evolution of the springtime transition in the stratosphere (Hardiman et al., 2011).

Figure 1 shows the vertical profile of the SFW dates for the (a) 1-hPa first, (b) 10-hPa first, and (c) neutral cases. The four CESM (WACCM) experiments are considered together. For 1-hPa first SFWs, the polar vortex initially breaks near the stratopause (i.e., at 1 hPa). In CESM (WACCM), the average timing of the SFW onset at 1 hPa is found on 22 April (±1.5 days; Figure 1a). This is consistent with the average SFW timing found in ERA-I (20 April; ±13.3 days). On average, the vortex breakup date propagates downward progressively from 1 to 30 hPa in ~20 days in both model and reanalysis. For the 10-hPa first SFWs (Figure 1b), the average timing of SFW onset at 10 hPa in CESM (WACCM) is found on 19 April (±5.9 days; i.e., 19 April 19) and shows a comparatively slower downward propagation (i.e., 16 days from 10 to 30 hPa). The average onset of 10-hPa first SFWs is found to occur significantly earlier in ERA-I, on 10 April (±1.9 days). It is

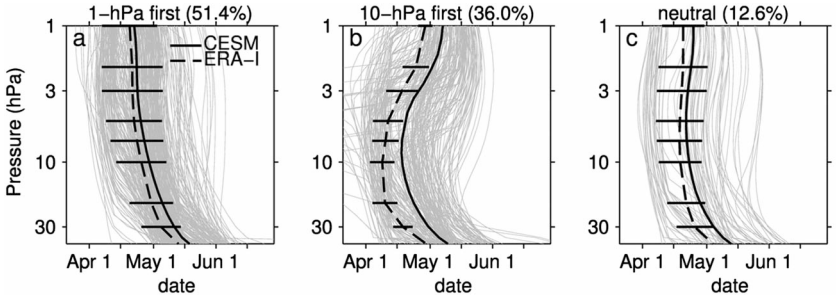


**Figure 1.** Vertical profile of the vortex breakup date (see text for details) for all final warmings simulated by the model (480 in total, thin gray profiles) classified as (a) 1-hPa first, (b) 10-hPa first, and (c) neutral. The solid (dashed) black line indicates the average of all profiles for the model (ERA-I reanalysis). Error bars indicate the $2\sigma$ standard error from the mean for ERA-I. CESM = Community Earth System Model.

noteworthy that SFW onsets (i.e., at 10 hPa on Figure 1a and 1 hPa on Figure 1b) exhibit a bimodal distribution with early and late clusters (see section 4 for further discussion).

In CESM (WACCM) simulations, 1-hPa first SFWs occur (51.4% or 298 cases in total) more frequently than 10-hPa first SFWs (36% or 209 cases in total). A similar distribution is found in the EMAC-O simulation with 56% of 1-hPa first and 32% of 10-hPa first SFWs (not shown). This contrasts with ERA-I results that revealed statistically significantly more frequent 10-hPa first SFWs (~55%). Finally, in simulations of both models (CESM [WACCM] and EMAC-O), around 12% of SFWs were classified as neutral SFWs and are not considered thereafter.

We then perform a composite analysis to examine the atmospheric circulation perturbations and responses associated with both types of SFWs (1-hPa and 10-hPa first). The central dates of the SFWs are defined as the vortex breakup date (see Figure 1) at the 1- and 10-hPa levels for the 1-hPa and 10-hPa first cases, respectively. The composites for a given SFW type are constructed by averaging the fields and/or field anomalies derived for each SFW of the same type. Here, monthly/daily *anomaly* refers to *deviation from the corresponding calendar monthly/daily climatology*. The statistical significance of the composites is estimated using a bootstrapping technique; that is, random sampling with replacement (Mudelsee, 2014). The procedure is to select a random subset from the original time-dependent data set with the number of samples equal to the original composite subset. More specifically, the original SFW onset dates are preserved but years are shuffled randomly. We reiterate this selection procedure 1,000 times to build a probability density function, which is then used to determine the likelihood of the derived signals to arise by chance. For two-dimensional fields, the procedure is done at each grid point independently. Two-tailed tests are employed.

To explore the influence of the wintertime dynamical evolution on the following springtime SFW characteristics, the frequency and timing of SSWs are analyzed. SSWs are identified by the simultaneous reversals of the zonal mean zonal wind at 10 hPa and 60°N and the zonal mean temperature difference between 60°N and the pole (Labitzke, 1981). Note that these particular criteria define *Major* SSWs, which we thereafter refer simply to as SSWs. The winter season is defined from 1 November to 15 days before the SFW central date in order to avoid any overlap between the SFW and SSWs.

## 3. Dynamical Evolution During SFWs

We first examine the stratospheric dynamics and the surface climate response associated with the 10-hPa and 1-hPa first SFWs in the four CESM (WACCM) model simulations. Note that in sections 3 and 4, the composite analysis combines all experiments averaged together as the atmospheric dynamical changes associated with the SFW lifecycle were found to be nearly independent of the experimental setting.

### 3.1. Stratospheric Dynamics

Figure 2 shows the anomalous stratospheric dynamical state for 10 days before the onset of the 10-hPa and 1-hPa first SFWs. Before the onset of 10-hPa first SFWs (Figure 2a), the zonal mean zonal wind anomalies are negative throughout the depth of the polar stratosphere (northward of 60°N) with a minimum of

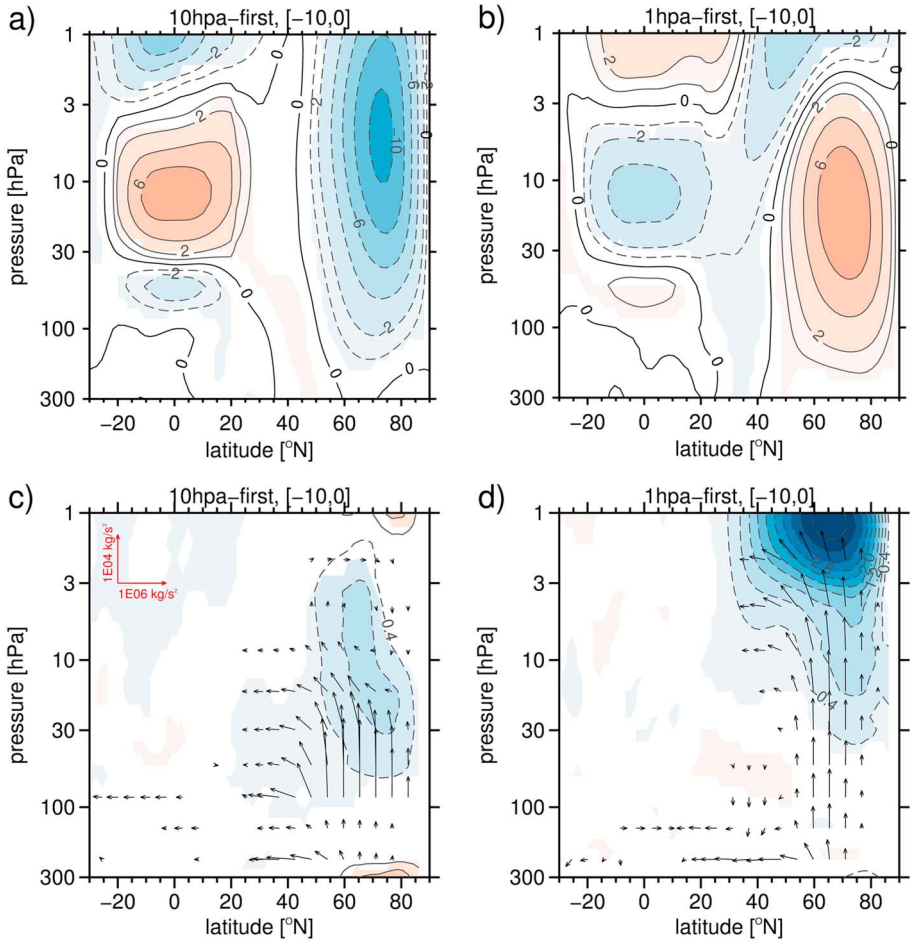


**Figure 2.** Zonal mean zonal wind anomaly (contour, drawn every 2 m/s) associated with the (a) 10-hPa first and (b) 1-hPa first cases averaged from −10 to 0 days relative to the stratospheric final warming central date. (c, d) As for (a) and (b) but for the Eliassen-Palm flux (vectors, scales and units are shown on the upper left of each panel) and its divergence (contours, drawn every 0.4 $m{\cdot}s^{-1}{\cdot}day^{-1}$) anomalies. Shading indicates regions where anomalies are statistically different from zero at the 95% confidence level.

−10 m/s centered at 75°N and 5 hPa (~40 km). This clearly indicates an anomalously weak polar vortex before the SFWs. Conversely, the 1-hPa first cases display positive zonal mean zonal wind anomalies in the polar stratosphere up to 3 hPa before the SFW, denoting an anomalously strong polar vortex, and negative values higher up that represent the start of the polar vortex breakup (Figure 2b). In the tropical stratosphere, for the 10-hPa first case, the zonal-mean zonal wind anomalies show anomalous westerlies centered at 20 hPa (6 m/s) and anomalous easterlies at about 50 hPa (−2 m/s). In the 1-hPa first case, the opposite pattern (but with a reduced magnitude) is found with anomalous easterlies at 20 hPa (−4 m/s) and westerlies at 50 hPa (1 m/s). The identification of this zonal-mean zonal wind dipole pattern in the tropical stratosphere hence would suggest a possible influence of the phase of the QBO on the SFW type in CESM (WACCM).

Figures 2c and 2d show the anomalies of planetary wave propagation and wave mean-flow interactions diagnosed by the Eliassen-Palm flux (EPF, vectors) and its divergence (contour). Recall that an anomalous convergence of EPF (or negative anomaly) leads to an enhanced wave drag and thus a relative westward acceleration of the zonal flow (i.e., a net deceleration of the westerly flow). Before the 10-hPa first SFW (Figure 2c), an anomalous increase in upward wave propagation is seen at high latitudes in the stratosphere. This increase in wave activity triggers an anomalous EPF convergence (i.e. enhanced wave breaking), which maximizes (0.8 $m{\cdot}s^{-1}{\cdot}day^{-1}$) near 75°N between 30 and 5 hPa. The wave-induced westward acceleration at these altitudes hence favors the westerly-to-easterly reversal of the wind that defines 10-hPa first SFWs. For

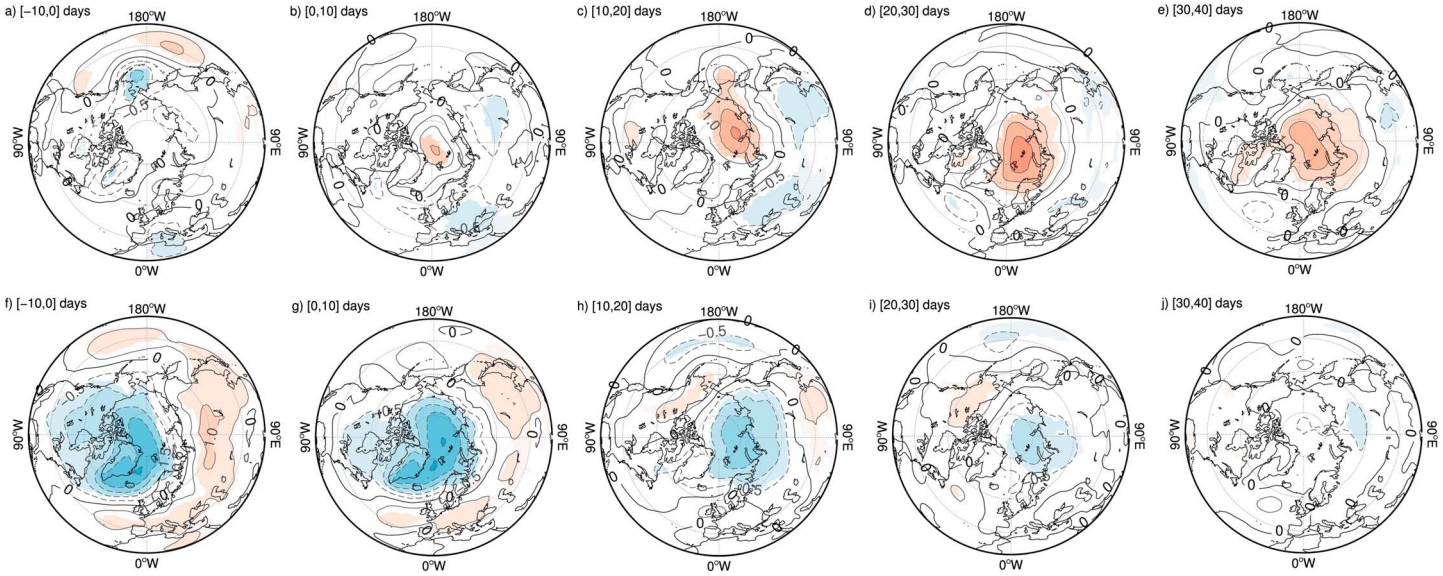


**Figure 3.** Sea level pressure anomaly associated with the 10-hPa first cases (a–e) and 1-hPa first cases (f–j) averaged in the ranges [-10,0], [0,10], [10,20], [20,30], and [30,40] days relative to the stratospheric final warming central date. All experiments are considered together. Contours are drawn every 0.5 hPa. Shading indicates regions where anomalies are statistically different from 0 at the 95% confidence level.

the 1-hPa first SFWs, the wave activity anomaly entering the stratosphere is stronger and concentrates in a narrower latitude band, which is centered at 65°N (Figure 2d). In comparison with the 10-hPa first cases, the EPF convergence anomaly for the 1-hPa first cases is also substantially larger (greater than 2 $m \cdot s^{-1} \cdot day^{-1}$) and localized at higher levels (above 3 hPa), in the stratopause region. This is consistent with the negative zonal mean zonal wind anomalies found in the upper polar stratosphere (Figure 2b).

The stratospheric dynamical characteristics prior to SFWs in our simulations are found to be consistent with Hardiman et al. (2011), which were based on the ERA-I reanalysis data set. Their analysis further revealed that SFWs were followed by significant perturbations of the tropospheric circulation. The following section focuses on the surface signals associated with the different SFW types and their effect on regional climate in our CESM (WACCM) simulations.

### 3.2. Surface Signals

The evolution of the 10-day average sea level pressure (SLP) anomalies around the onset of the SFWs is shown in Figure 3. No significant SLP signal is found during the period preceding 10-hPa first SFWs (Figure 3a). Within the 10 days following 10-hPa first SFWs (Figure 3b), a high-pressure anomaly (greater than 1 hPa) starts to develop over the polar cap, accompanied with low pressure anomalies over Europe and East Asia. The high-pressure anomaly then further enlarges and persists throughout the following month (Figures 3c–3e), while the low-pressure anomalies vanish earlier (days 20–30; Figure 3d). The evolution of the SLP anomalies associated with 1-hPa first SFWs differs markedly. Before the onset of 1-hPa first SFWs (Figure 3f), the SLP signal shows clear negative anomalies extending over the polar cap and Greenland and positive anomalies at mid-latitudes that encompass the East Atlantic-European sector, Northern Asia, and the North Pacific. This pattern, which strongly resembles the positive phase of the Arctic Oscillation, then progressively vanishes within the month following the 1-hPa first SFW (Figures 3g–3j). Note that for both types of SFWs, the SLP anomaly evolves similarly (toward a more negative North Atlantic/Arctic Oscillation) despite different tropospheric initial situations as shown by the temporal evolution of Figures 3a-to-3e and Figures 3f-to-3j. Hence, this suggests that there are no different stratosphere-troposphere processes at work between the two types of SFWs.

A similar SLP analysis has also been conducted with the EMAC-O simulation and ERA-I data (Figures S1 and S2). EMAC-O results show a temporal and spatial response consistent with that of CESM (WACCM) but with reduced statistical significance. In ERA-I, although the anomalies appeared consistent with those

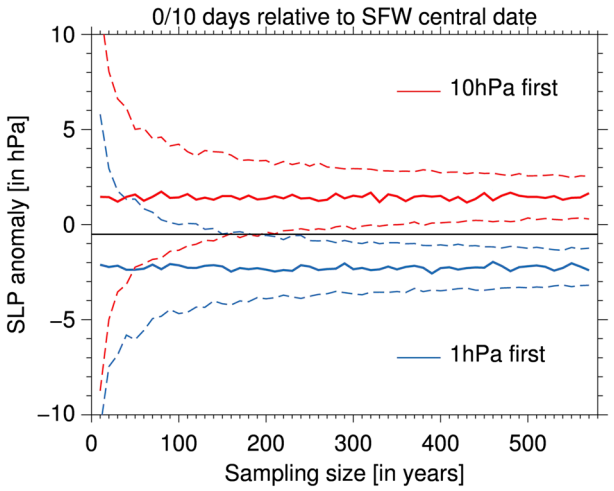


**Figure 4.** SLP anomalies averaged northward of 85°N and from 0 to 10 days after the SFW onset as a function of the number of years sampled. Each is based on 1,000 random realizations. The solid line shows the average and the dashed line the 2.5th and 97.5th percentiles. The horizontal line at −0.5 hPa indicates the climatological anomaly of SLP averaged from 0 to 10 days before SFW onset, regardless of their type. SFW = stratospheric final warming; SLsea level pressure.

of CESM (WACCM) for the 1-hPa first cases, the statistical significance is substantially reduced. For the 10-hPa first cases, while some statistically significant polar positive signal is found at lag-10 to zero, no statistically significant signal could be identified after lag zero. This suggests that, at this 10-day timescale, a relatively large sample is required for the signal to be identified and overcome the large interannual variability. We examined the effect of the sampling size on the strength of the signal and its significance in our CESM (WACCM) experiments. Figure 4 shows how the sampling size (number of years used to perform the composite analysis) affects the SLP anomaly signal averaged northward of 85°N and from 0 to 10 days relative to the SFW onset (corresponding to panels b and g of Figure 3). For each sample size $n$ (spanning from 10 to 570 years by increment of 10 years), we randomly select $n$ years from which we calculate the 1-hPa and 10-hPa first composite anomalies. This procedure is repeated 1,000 times for each $n$, allowing to construct distributions of the average composite values. The results show that a sample of more than ~200 years is needed to have a more than 97.5% chance to obtain averaged SLP anomalies 10 days after 10-hPa first (red) and 1-hPa first (blue) SFWs that are different from the climatological anomaly associated with SFWs. Even if the model and reanalysis are not directly comparable since the SLP variability and the frequency of 10-hPa and 1-hPa first SFW years are different, these results suggest that large samples are needed to obtain a robust SLP signal associated with the type of SFW and may partly explain why the signals are not well identified in the ~40 years of the ERA-I data set.

Although the analysis of the signals relative to the central date of SFWs provides relevant insights regarding the dynamical evolution of the near-surface circulation associated with SFWs, it does not quantify the subseasonal surface climate signals associated with SFWs that are important for seasonal forecasts. We now examine the differences in springtime SLP and surface temperature anomalies between years featuring 1-hPa first SFW and years featuring 10-hPa first SFW. Results for April and May are shown in Figure 5.

In April (Figure 5a), the SLP mean difference between 10-hPa and 1-hPa first SFWs reveals a pattern similar to the negative phase of the NAO/Arctic Oscillation, with a maximum positive pressure anomaly greater than 3 hPa over the polar cap/Greenland and minimum pressure anomalies of −1 hPa at midlatitudes. These atmospheric circulation perturbations lead to substantial surface temperature changes at regional scale with cold anomalies lower than −1 K over Northern Eurasia, and moderate (but statistically significant) warm anomalies over Greenland and Southern Eurasia (Figure 5c). Note that excluding years where SFWs occur in May from these April composites (Figures 5a and 5c) does not significantly affect the results on the surface response (not shown). In May, similar but weaker responses are found in SLP (Figure 5b) and surface temperature (Figure 5d). CESM (WACCM) results are consistent with EMAC-O (Figure S3a) and ERA-I (Hardiman et al., 2011), which reveal similar NAO-like signals in April when 1-hPa first SFW years are compared to 10-hPa first SFW years.

Atmospheric circulation changes associated with the NAO affect the underlying Atlantic Ocean by modulating surface air temperature, atmosphere-ocean heat fluxes, and midlatitude wind stress (Visbeck et al., 2003). This induces SST anomalies that we examined in Figures 5e and 5f. In April (Figure 5e), the SST signal is characterized by warm anomalies in the North Atlantic (50–60°N) and subtropical North Atlantic (~30°N), and cold anomalies at midlatitudes (~40°N). This tripolar SST pattern agrees well with the typical oceanic response to negative NAO-like atmospheric anomalies (Czaja & Frankignoul, 2002). In May (Figure 5f), a similar SST signal is found which is further amplified at mid and high latitudes. Nevertheless, the statistical significance of this SST tripole is relatively weak despite the large sample (435 years since the FixedSST experiment is not included). This may partly explain the absence of a SST signal in observations (not shown).

In this section, we have shown that the two different types of SFWs are associated with significant regional climate perturbations in the Northern Hemisphere, which may contribute to a better

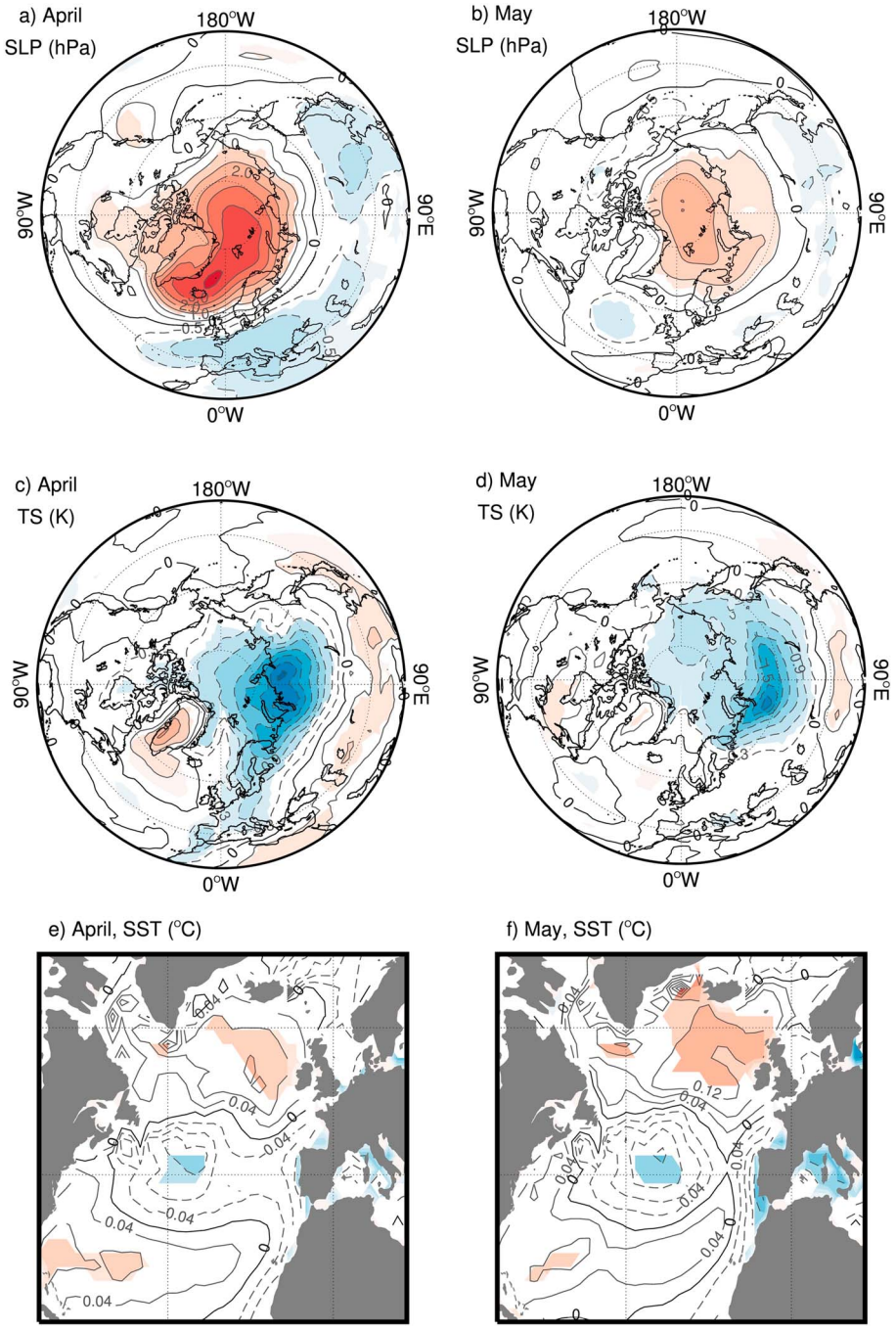


**Figure 5.** Difference between 10-hPa and 1-hPa first years of the (a, b) sea level pressure (SLP), (c, d) air surface temperature, and (e, f) SSTs in (a, c, and e) April and (b, d, and f) May. All experiments are considered together, except for (e, f) where FixedSST is discarded. Contours are drawn every (a, b) 0.5 hPa, (c, d) 0.3 K, and (e, f) 0.04 K. Shading indicates regions where differences are statistically significant at the 95% confidence level. SST = sea surface temperature.

understanding of interannual climate variability in spring. Given the remarkable different stratospheric dynamical conditions preceding the two types of SFWs (e.g., Figure 2), we further examine in the next sections whether the stratospheric dynamical evolution throughout the previous winter and the influence of external stratospheric variability factors can provide insights on the spring SFW transition. In other words, can we identify a stratospheric preconditioning that helps to predict the type of SFW?

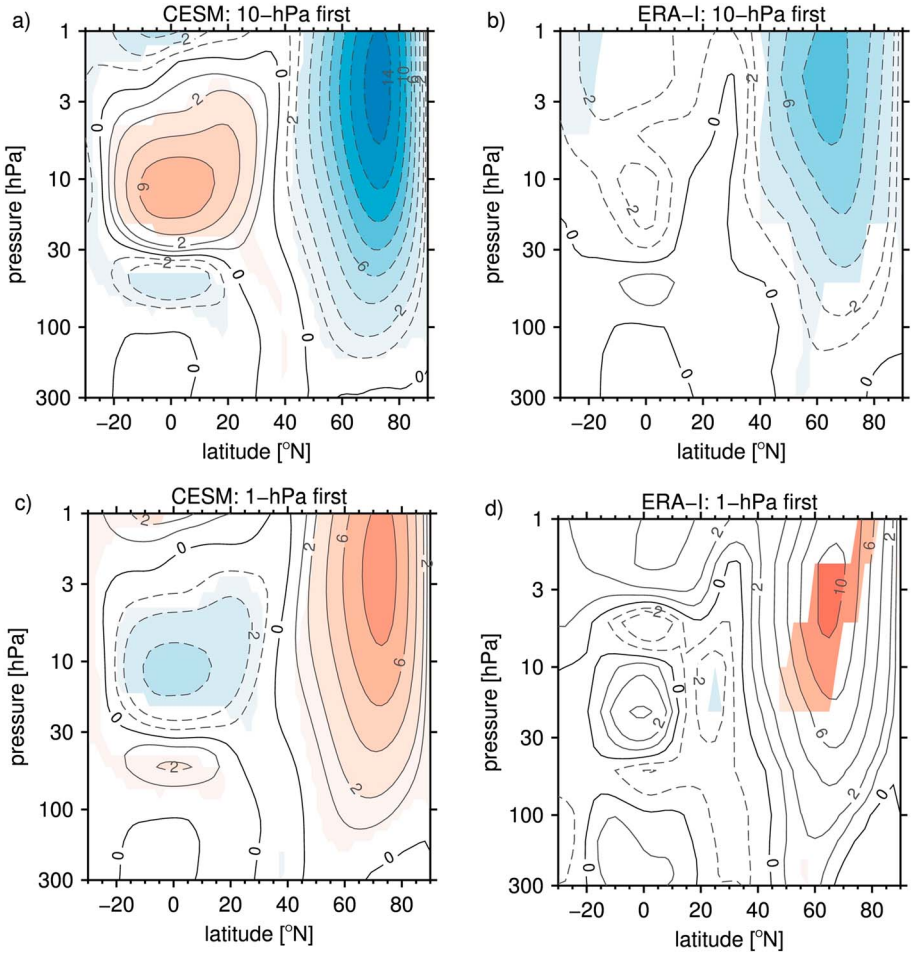


**Figure 6.** Composites of zonal-mean zonal wind anomalies in March for the (a, b) 1-hPa first and (c, d) 10-hPa first stratospheric final warming years. Panels (a) and (c) and (b) and (d) show CESM (Whole Atmosphere Community Climate Model) and ERA-Interim results, respectively. Shading indicates regions where anomalies are statistically different from the climatology at the 95% confidence level. CESM = Community Earth System Model.

## 4. Influence of Preceding Winter on SFWs

To investigate the stratospheric dynamical preconditioning, we first analyze the zonal flow anomalies in late winter preceding 1-hPa and 10-hPa first SFWs. Figure 6 shows the zonal-mean zonal wind anomalies in March associated with 1-hPa and 10-hPa first SFWs in CESM (WACCM) and ERA-Interim. Statistically significant strong westerly anomalies, in excess of 5 m/s from 30 to 1 hPa, are found in the polar stratosphere in March for years featuring 1-hPa first SFWs (Figures 6a and 6b). This finding is robust across CESM (WACCM) and ERA-Interim (and EMAC-O; see Figure S4), supporting that the polar vortex is anomalously strong during the late-winter period which precedes 1-hPa first SFWs. Inversely, the polar vortex preceding 10-hPa first SFWs is anomalously weak as revealed by the strong and significant easterly anomalies (Figures 6c and 6d). Note that, for February, we consistently found an anomalously strong (weak) polar vortex strength associated with 1-hPa first (10-hPa first) SFWs in CESM (WACCM) and EMAC-O (not shown).

In the tropical stratosphere, the zonal mean zonal wind anomalies associated with SFW types markedly differ between CESM (WACCM) and reanalysis. CESM (WACCM) composites show that the tropical stratosphere for 1-hPa SFWs is dominated by easterly anomalies at 10 hPa and westerly anomalies at 50 hPa (Figure 6c), and the opposite for 10-hPa SFWs (Figure 6a). Note that this tropical zonal wind anomaly pattern is found in the three CESM (WACCM) sensitivity experiments with a nudged QBO (i.e., Natural, RCP85, and FixedSST) when they are analyzed separately (not shown). This indicates that, in CESM (WACCM) simulations, the easterly (westerly) phase of the QBO (defined at 50 hPa) favor 10-hPa (1-hPa)

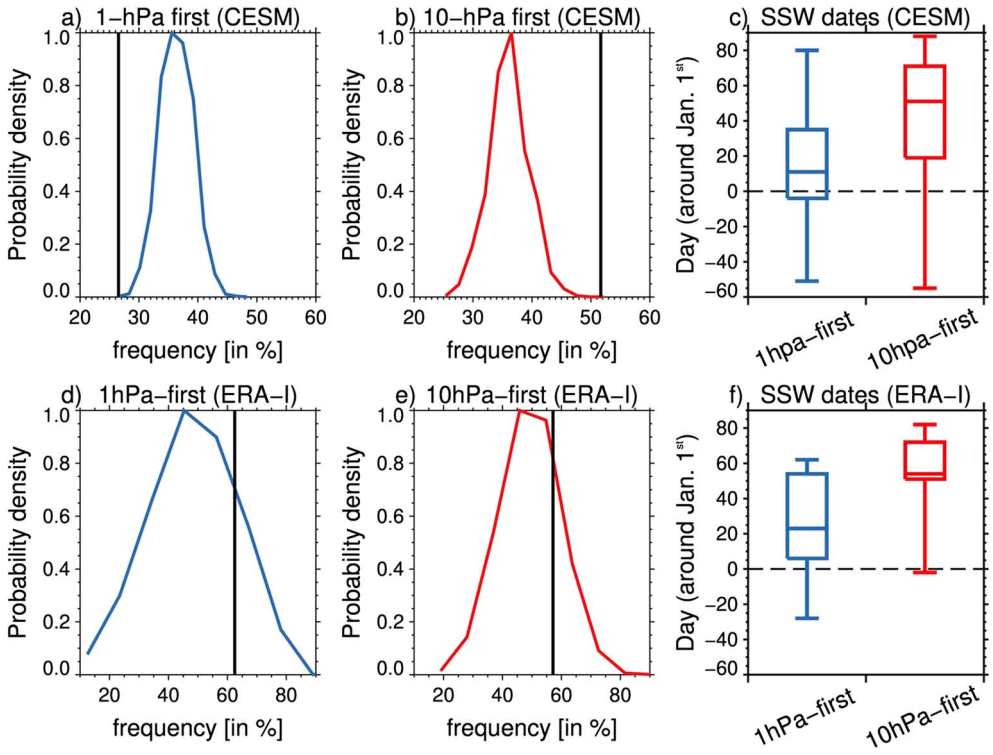


**Figure 7.** (a, b, d, and e) Monte Carlo test of the likelihood (expressed in percent) that at least one SSW occurred during winter using 10,000 synthetic time series generated with random assignments of the SFW type but preserving the same number of years in each group (i.e., [b] 209 for 10-hPa first and [a] 298 for 1-hPa first in CESM [WACCM]) among the total number of years (i.e., 580). The vertical solid line indicates the likelihood when the (a, d) 1-hPa and (b, e) 10-hPa first years are sampled separately. (c, f) Box diagram of the SSW central date (see text for details) for the 1-hPa and 10-hPa first cases. The center line, box edges, and whiskers indicate the median, first and third quartiles, and extreme values, respectively. Panels (a)–(c) and (d)–(f) show CESM (WACCM) and ERA-Interim results, respectively. SSW = sudden stratospheric warming; WACCM = Whole Atmosphere Community Climate Model.

first SFWs. In contrast, no such preceding QBO-like signature is found in relation with either the 10-hPa or 1-hPa SFW type in ERA-interim. In the same way, EMAC-O results do not show evidence of a link between the QBO phase and the type of SFWs (Figure S4). The relationship between the QBO phase and the type of SFWs, found in CESM (WACCM) results, is thus not a robust feature, clearly showing model dependency.

Given the relationship between the preceding polar vortex strength in late winter and the type of SFW later on, any factor modulating the polar vortex in winter may thus indirectly affect the occurrence and timing of spring SFWs. Since SSWs are the primary driver of polar vortex strength variability in winter, we now investigate whether there is a relationship between their occurrence in winter and the type of SFWs in spring.

Figure 7 examines the link between SSW characteristics (i.e., frequency and timing) and the type of SFW for CESM (WACCM) and ERA-I. As shown by the probability distributions, if SFW years are sampled randomly (i.e., independently of the SFW type), there is a climatological probability of ~37% to have at least 1 SSW per winter in CESM (WACCM; peak of the distributions in Figures 7a and 7b) and ~50% in ERA-I (peak of the distribution in Figures 7d and 7e). Note that the large difference between CESM (WACCM) and ERA-I is consistent with the anomalously strong polar vortex (also referred to as “cold pole bias”) in CESM (WACCM), which makes SSWs less frequent (Marsh et al., 2013). If, instead, the sampled years are not randomly distributed but defined according to the nature of the SFW, the chances that at least 1 SSW occurs over the previous winter decrease to 26% in CESM (WACCM) for the 1-hPa first case (vertical line in Figure 7a) and increase to 52% in CESM (WACCM) for the 10-hPa first case (vertical line in Figure 7b). These probability frequencies are significantly different from the climatological likelihood at the 95% confidence level. This indicates that, for the SFW years in our CESM simulations, winters with and without SSW are more likely to be followed by 10-hPa and 1-hPa first SFWs, respectively. Such a relationship is also found

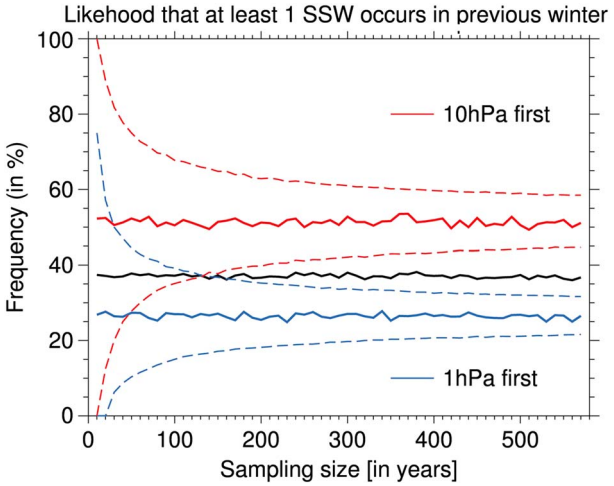


**Figure 8.** Probability that at least 1 SSW occurs in the previous winter for (black) random years sampling, (red) 10-hPa first years sampling, and (blue) 1-hPa first years sampling as a function of the number years considered. Each is based on 1,000 random realizations. The solid line shows the average and the dashed line the 2.5th and 97.5th percentiles. SSW = sudden stratospheric warming.

in EMAC-O results (see Figure S5). In CESM (WACCM), winters featuring more than one SSW occurrence further increase the likelihood of a 10-hPa first SFW to occur in spring (not shown).

As shown in Figure 1, SFW onsets reveal a bimodal distribution with early and late dates. We investigate the possible causes of this bimodal structure by separating each SFW type according to the timing of their onset. We hence define four clusters: early 10-hPa first, late 10-hPa first, early 1-hPa first, and late 1-hPa first SFWs. By repeating the analysis of Figures 7a and 7b, we find (not shown) that late 10-hPa first SFWs are associated with a probability of SSWs even higher (60% instead of 52%) than when all 10-hPa first SFWs are considered. The opposite is found for early 1-hPa first SFWs with a decrease in the frequency of SSWs (20% instead of 26%). This suggests that SSW occurrences in previous winter not only affect SFW types but can additionally influence the timing of the SFW as suggested by Hu et al. (2014).

Inversely, the timing of the SSWs also impacts the type of SFW. Figure 7c shows the distribution of central dates of SSWs preceding 1-hPa (blue) and 10-hPa (red) SFWs in CESM (WACCM). Note that if several SSWs occur over one winter, only the central date of the latest one is included in the distribution. This analysis demonstrates that SSWs recorded in winters preceding 1-hPa first SFWs are more likely to occur significantly earlier in the season than for the case of 10-hPa first SFWs. Again, this finding is confirmed with EMAC-O results (see Figure S5). Hence when a SSW occurs in early winter, despite the partial breakup of the polar vortex, the relatively long time lapse before spring allows the recovery of a strong polar vortex (through radiative processes), which thus favors the occurrence of 1-hPa first SFW. In contrast, if a SSW occurs in late winter, the polar vortex recovery through radiative processes is less efficient since the meridional gradient of the net radiative heating is less pronounced (e.g., Mlynczak et al., 1999). As a consequence, the polar vortex is more likely to remain weak until spring, hence favoring the occurrence of 10-hPa first SFW.

We also examine the link between the occurrence of SSWs in winter and the type of SFW using ERA-I, but no relationship is found (Figures 7d and 7e). Analogously to the SLP analysis presented in section 3, we test the influence of the sampling size on the statistical significance of the relationship between SSWs in winter and the type of SFW using CESM (WACCM) data. Results are shown in Figure 8. As expected, the spread of the probability distribution that at least 1 SSW occurs before each type of SFW decreases with increasing sample size. The results also suggest that samples of more than 150 years are required to have more than 97.5% likelihood that the frequencies of SSWs before 10-hPa first (red) and 1-hPa first (blue) cases differ from the climatological frequency (i.e., 37%). The relatively short period covered by ERA-I may thus partly explain the absence of detection of SSW-/SFW-type relationships. Nonetheless, analysis of ERA-I suggests a relationship between the SSW timing and the SFW type, which is consistent with the model results (Figure 7f): SSWs recorded in winter preceding 1-hPa first SFWs are more likely to occur earlier in the season than for the case of 10-hPa first SFWs.

In this section, model results demonstrate that the dynamical variability of the polar stratosphere during winter has a significant impact on the development of SFW recorded later in spring. The next section focuses on the influence of external sources of variability and forcings on SFW.

## 5. Influence of Remote Variability Sources on SFWs

As developed in the introduction, it is well established that the stratospheric polar vortex can be influenced by external variability sources such as, for example, ENSO, QBO, or anthropogenic emissions. Since we demonstrated in the previous section that the type of SFW is significantly connected to the strength of the polar vortex, SFW variability should also be linked to these external variability sources. In this regard, we now examine the influence of the different experimental settings (i.e., FixedSST, NoQBO, and RCP85) on SFWs in the CESM (WACCM) simulations.

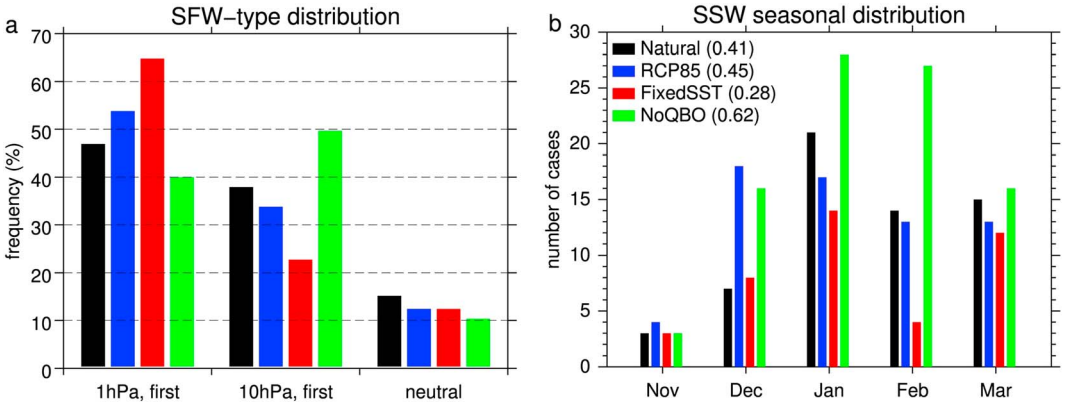


**Figure 9.** (a) Distribution of SFWs and (b) seasonal distribution of SSWs in the (black) Natural, (blue) RCP85, (red) FixedSST, and (green) NoQBO experiments. SFW = stratospheric final warming; SSW = sudden stratospheric warming.

### 5.1. Frequency

Figure 9a shows the distribution of the SFW type as a function of the experimental setting. The most important differences in SFW distribution with respect to the Natural experiment are found in the FixedSST and NoQBO simulations. Removing the interannual SST variability in the FixedSST experiment leads to an 18% increase in the 1-hPa first SFW frequency and a decrease of 17% in 10-hPa first SFWs frequency compared to the Natural experiment. This difference is statistically significant at the 95% level according to the $\chi^2$ test. Conversely, removing the QBO variability in the NoQBO experiment results in a 7% decrease in the 1-hPa first SFW frequency and a 12% increase in the 10-hPa first SFWs frequency compared to the Natural experiment (significant at the 90% level). Note that the NoQBO experiment is the only simulation showing more frequent 10-hPa first than 1-hPa first SFWs (+10%). The NoQBO SFW distribution is significantly different from the FixedSST one at the 99% confidence level. The RCP85 SFW distribution shows no statistically significant difference with the Natural experiment. We further investigated whether the distribution of SFWs in the RCP85 could change in time but no significant trend was found. Note that an averaged frequency of ~12% of neutral SFWs is found, independently of the experimental setting.

Given the relationship found between the type of SFW and the occurrence of SSWs in the preceding winter (Figure 7), we investigate the influence of the remote variability sources on SSWs. Figure 9b shows the seasonal distribution of SSWs for the four different experiments. Overall, removing the QBO leads to a substantial increase of SSW frequency (6.2 SSWs/decade in the NoQBO experiment compared to 4.1 SSWs/decade in the Natural experiment), while removing the inter-annual SST variability leads to a decrease of SSWs frequency (2.8 SSWs/decade in the FixedSST experiment) as noticed by Lubis, Matthes, et al. (2016). The most pronounced differences in SSW frequency between the experiments are found in December, January, and February (DJF), which correspond to the months when SSW have a prominent impact on the type of SFWs (Figure 7c). The changes in the number of SSW events with respect to the Natural experiment are consistent with the changes in the type of SFW. In the NoQBO experiment, the important increase of SSW events in DJF is, as expected, accompanied with an enhanced occurrence of 10-hPa first SFWs. In the FixedSST experiment, the dramatic reduction of SSWs in winter (particularly pronounced in February) is also consistent with the enhanced occurrence of 1-hPa first SFWs and reduced occurrence of 10-hPa first SFWs.

The influence of the external variability sources on the seasonal climatological evolution of the extratropical zonal mean zonal wind is further investigated in Figure 10. It shows the differences between the FixedSST (panel a), NoQBO (panel b), or RCP85 (panel c) simulations and the Natural experiment. Constraining the model with climatological SSTs (Figure 10a) leads to a substantial strengthening of the polar vortex, which is particularly pronounced in late winter/early spring with differences greater than 4 m/s from January to April between the Natural and FixedSST experiments. These strong vortex anomalies during this period are in turn consistent with the significant increase (decrease) of 1-hPa (10-hPa) first SFWs in the FixedSST experiment. Note that the stronger and hence less disturbed polar vortex in the FixedSST

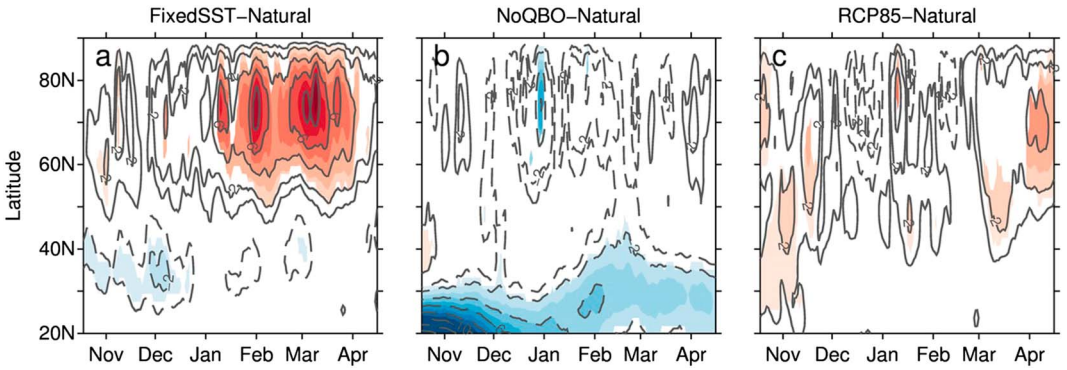


**Figure 10.** Differences of daily climatology of 10-hPa zonal mean zonal wind from November to April in the Northern Hemisphere between (a) FixedSST, (b) NoQBO, (c) RCP85, and the Natural experiments. Solid (dashed) contours indicate positive (negative) anomalies and are shown with intervals of 1 m/s. Shading indicates that differences are statistically significant at the 95% confidence level (two-tailed Student's *t* test).

experiment is consistent with missing variability sources in the troposphere, which results in reduced upward wave propagation and decreased wave dissipation/breaking in the stratosphere (see Figure S1 in Lubis, Matthes, et al., 2016).

Removing the QBO nudging (i.e., resulting in constant weak easterlies in the tropical lower stratosphere on average) is found to have less impact on the polar night jet strength than removing interannually variable SSTs (Figure 10b). In the NoQBO experiment, the polar night jet appears climatologically weaker than in the Natural experiment in midwinter (i.e., DJF) but the differences are only marginally significant. In spring, no differences are found between both experiments.

The polar night jet anomalies associated with the RCP85 scenario show an overall strengthening (Figure 10c), which is statistically significant in early winter (i.e., October/November) and spring (i.e., March/April). These two periods of seasonal transitions in the stratosphere—when the polar vortex forms and breaks up—are particularly sensitive to radiative effects. Despite the absence of significant effects of these polar vortex changes on the distribution of SFW type (Figure 9), these anomalies may still affect the timing of SFWs that we examine in the next part.

### 5.2. Timing

Previously we showed that in CESM (WACCM) the SFW onset occurs on average on 22 and 19 April for 1-hPa first and 10-hPa first cases, respectively (Figure 1). As shown in Figure 11, the timing of SFWs is, however, sensitive to natural and anthropogenic external drivers. In the Natural and RCP85 experiments, 10-hPa first SFWs occur on average 7–8 days earlier than 1-hPa first SFWs. This behavior is consistent with reanalysis results (see Figure 1). The early occurrence of 10-hPa first SFWs compared to 1-hPa first SFWs is also seen in the FixedSST experiment, although the timing difference is substantially reduced and not statistically significant. Finally, in the NoQBO experiment, there is no difference in the averaged timing of both types of SFWs. Furthermore, on average, 10-hPa first SFWs occur later in the NoQBO experiment and 1-hPa first SFWs occur earlier in the FixedSST experiment in comparison with the Natural and RCP85 experiments. As mentioned in section 4, we find that SSW occurrences not only affect SFW types but can also influence their timing: late 10-hPa first (early 1-hPa first) SFWs are associated with a higher (lower) probability of SSWs occurrence in the previous winter, respectively. The anomalously high frequency of SSWs in the NoQBO experiment may hence lead to favor late 10-hPa first SFWs, while the anomalous low frequency of SSWs in the FixedSST experiment may rather favor early 1-hPa first SFWs.

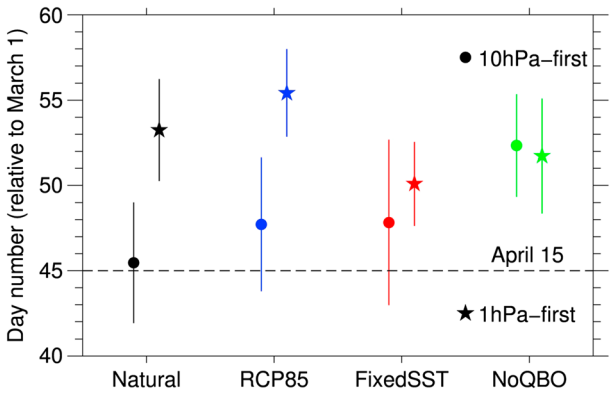


**Figure 11.** Averaged timing (number of days since 1 March) of the (star) 1-hPa first and (dots) 10-hPa first stratospheric final warmings for the four Community Earth System Model (Whole Atmosphere Community Climate Model) experiments. Bars indicate the 2-$\sigma$ confidence intervals. Horizontal dashed line indicates the day number corresponding to 15 April.

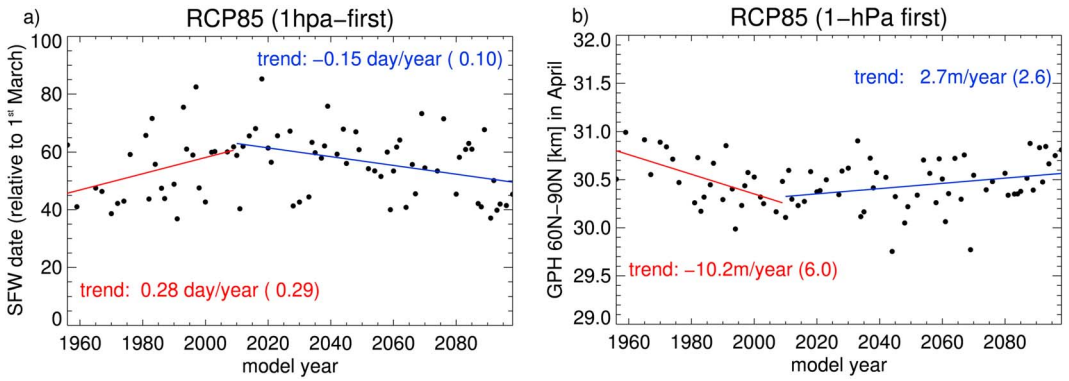


**Figure 12.** Annual evolution of (a) the 1-hPa first SFWs timing and (b) the April polar cap mean geopotential height for years associated with 1-hPa first SFWs in the RCP85 experiment. Brackets indicate the 2-$\sigma$ error of the trend estimate. SFW = stratospheric final warming; GPH = geopotential height.

An additional noticeable difference in the SFWs averaged timing is the anomalously late 1-hPa first SFWs found in the RCP85 experiment (Figure 11), which is consistent with the climatologically stronger polar westerly anomalies found in April (Figure 10c), and which should be related to changes in ODS and/or GHG concentrations.

Figure 12 shows the time evolution of the SFW timing (panel a) and the geopotential height (panel b) over the polar cap at 10 hPa in April for the years with a 1-hPa first SFW for the RCP85 experiment. The 1-hPa first SFW timing is not stationary over time. Our results rather suggest that from 1955 to 2010 (2010 to 2099), 1-hPa first SFWs tend to occur increasingly later (earlier) in spring as indicated by the positive (negative) trend of ~3 days (−1.5 days) per decade (Figure 12a). This piecewise SFW timing evolution is consistent with the evolution of the polar vortex strength in April as diagnosed by the geopotential height (Figure 12b), which shows that the spring polar vortex gradually strengthens (weakens) before (after) 2010. Note that this piecewise evolution is not found for both types of SFWs in the Natural, NoQBO, and FixedSST experiments and not found either for 10-hPa first SFWs in the RCP85 experiment (not shown). Furthermore, the inflection period (near 2010) seems to coincide with the onset of the ozone recovery in the Northern Hemisphere in the RCP85 experiment (see Lubis, Omrani, et al., 2016, which shows the ozone recovery in this CESM (WACCM) RCP85 experiment). These results hence suggest that 1-hPa first SFW timing may be influenced by ODSs and related to long-term ozone changes.

## 6. Summary and Discussion

This study examines the dynamics, surface signals, and drivers of the variability of boreal SFWs based on multidecadal simulations of the CESM (WACCM) and EMAC-O models, and the ERA-Interim data set. SFWs are classified according to their vertical temporal development (Hardiman et al., 2011), that is, events can occur first in the midstratosphere (10-hPa first SFWs) or in the upper stratosphere (1-hPa first SFWs).

We demonstrate that the CESM (WACCM) and EMAC-O models are able to simulate both types of SFWs (i.e., 10-hPa and 1-hPa first) identified in reanalyses (Hardiman et al., 2011). However, both models simulate more frequent 1-hPa first SFWs (greater than 50%) than 10-hPa first SFWs (lower than 40%), in contrast to ERA-I that shows a vast majority of 10-hPa first SFWs (55%) against only 21% of 1-hPa first SFWs. We found that the type of SFW is linked to the polar vortex strength in March with 1-hPa/10-hPa first SFWs preceded by an anomalously strong/weak polar vortex. Given that the climatological polar vortex of both models is anomalously strong in late winter, it is likely that this contributes to the biased high frequency of 1-hPa first SFWs in models compared to reanalysis.

In springtime, CESM (WACCM) and EMAC-O simulations reveal a statistically significant surface signal associated with the SFW type, which projects onto a pattern resembling the AO/NAO as found in Hardiman et al. (2011) based on reanalysis data. In the CESM (WACCM) experiments, the NAO-like surface response to SFW variability is further associated with a tripolar SST pattern in the North Atlantic sector.

Note, however, that this SST anomaly is not detected in the reanalysis and the EMAC-O simulation, possibly because the number of years is too low to separate the SFW SST signal from other sources of ocean variability. Furthermore, the springtime SST tripole signature associated with the NAO index in EMAC-O appears much weaker than the one of CESM (WACCM), which may be indicative of reduced air-sea coupling intensity in EMAC-O (Figure S6).

Given the potential impact of SFW variability on the seasonal forecast, we then examined whether particular wintertime stratospheric conditions can influence SFWs. Notably, the very large number of model years allowed us to find that both SFW types are associated with specific characteristics in the occurrence of mid-winter SSWs. Both models reveal that winters with SSWs are more likely to be followed by 10-hPa SFWs, while winters without SSWs usually end up with 1-hPa SFWs. Furthermore, if a SSW is recorded in winters preceding 1-hPa first SFWs, the SSW is more likely to occur significantly earlier in the season than for the case of 10-hPa first SFWs. The link between SSW and SFW is only partially identified in ERA-I. Although we found that the ERA-I period seemed too short for deriving a statistically significant relationship between SSW occurrence and SFW types, possible shortcomings in the representation of stratospheric dynamical variability in the two models cannot be discarded. Note also that our results suggest that SSW occurrences in previous winter not only affect SFW types but can additionally influence the timing of the SFW in agreement with Hu et al. (2014).

The separate analysis of the CESM (WACCM) sensitivity experiments revealed that the interannual variability of SST and stratospheric equatorial winds has a substantial influence on the type of SFW. We found that removing interannually varying SSTs results in a climatological stronger polar vortex and a reduced number of SSWs, which in turn leads to a significant increase/decrease of the 1-hPa first/10-hPa first SFW frequency. Conversely, removing the QBO nudging in the tropical stratosphere (leading to relatively constant weak easterlies) induces an increase/decrease of the 10-hPa first/1-hPa first SFW frequency, which is consistent with the increased frequency of SSWs found in January/February (i.e., favoring 10-hPa first occurrence). This further agrees with the findings of Gray et al. (2004), based on idealized experiments, that showed that imposing easterlies at any height in the tropical stratosphere increases the frequency of SSWs. A link between the QBO phase and SFW frequency is not clear, however. In CESM (WACCM), we found that 10-hPa first SFWs are associated with equatorial westerly/easterly anomalies centered at 10/50 hPa and the opposite for 1-hPa SFWs. This appears consistent with the H-T relationship: that is, the easterly QBO phase (defined at 50 hPa) leads to a more disturbed polar vortex in winter, and hence to a higher chance of 10-hPa first SFW occuring in spring. Our CESM (WACCM) findings are however neither supported by ERA-I (our study or Hardiman et al., 2011) nor EMAC-O results. We performed additional analysis, which revealed a much weaker H-T effect in ERA-I and EMAC-O than in CESM (WACCM; not shown). This might be indicative of a model dependency of this relationship, which may be a consequence of the QBO nudging procedure. Further investigation based on experiments with an internally generated QBO would be necessary to test the robustness of the QBO/SFW relationship in CESM (WACCM).

Finally, the sensitivity of SFW characteristics to long-term changes in GHG and ozone depleting substance concentrations was investigated. While the distribution of SFW frequency appears not to be affected by these changes, their timing does. Namely, 1-hPa first SFWs tend to occur increasingly later/earlier before/after 2010 in the RCP85 CESM simulation, which is consistent with piecewise trends in the strength of the polar vortex in April. This change in 2010 also appears to correspond approximately to the change from ozone depletion to ozone recovery in the CESM simulation. Note that a similar relationship between late winter/early spring Arctic polar vortex strengthening and ozone depletion for years without winter major warmings was also identified by Ivy et al. (2014) based on reanalysis and observations. In contrast, we found no significant trend for 10-hPa first SFWs in the RCP85 experiment (not shown). As shown in our study, 1-hPa first SFWs are favored by anomalously strong vortex conditions in spring throughout the depth of the stratosphere. These strong vortex conditions in spring are expected to be further strengthened in an ozone depleting context (i.e., decreasing ozone leads to radiative cooling over the polar cap), which in turn can delay 1-hPa first SFWs. Such a relationship between vortex strength and its breakup timing in association with ozone depletion was already detected in the Southern Hemisphere (Waugh et al., 1999). This is not found for 10-hPa first SFWs since, in this case, the vortex is more perturbed by wave forcing over the preceding winter (i.e., increasing likelihood of SSW to occur), which in turn leads generally to a reduced ozone loss in spring (e.g., Kuttippurath & Nikulin, 2012). Although the analysis of additional and independent model

experiments is required to assess the robustness of this link, it may be an additional possible sign of the impact of ozone changes on Arctic stratosphere dynamical evolution, suggesting the potential importance of accounting for ozone-circulation feedback when simulating long-term stratosphere and climate evolution (Previdi & Polvani, 2014).

Overall, this model-based study provides a better understanding of the processes driving springtime dynamical variability of the boreal stratosphere and its connection with near-surface climate. As a final remark it is important to highlight that most of our main findings in this study could be determined thanks to the very large data set offered by the multiple model realizations that considerably enhanced the signal-to-noise ratio. This would not have been possible by restricting our study to reanalysis data solely.

**Acknowledgments**
This project was supported by the European Project StratoClim (7th framework programme, Grant agreement 603557) and the Grant "SOLSPEC" from the Centre d'Etude Spatiale (CNES). R. T. was supported by a grant from the LABEX L-IPSL (ANR-10-LABX-0018), funded by the French Agence Nationale de la Recherche under the "Programme d'Investissements d'Avenir." B. A. was supported by "Ayudas para la contratación de personal postdoctoral en formación en docencia e investigación en departamentos de la Universidad Complutense de Madrid." This study is based on work started at GEOMAR. The CESM (WACCM) simulations were performed at the Deutsche Klimarechenzentrum (DKRZ) Hamburg, Germany. We thank Steven Hardiman for helpful discussions. The source code of the Community Earth System Model version 1.0 (CESM 1.0) used in this study is publicly distributed and can be obtained after registration at http://www.cesm.ucar.edu/models/cesm1.0/ website. ERA-Interim data used in this study are available at http://apps.ecmwf.int/datasets/after registration website. The data from the CESM model experiments used in this study are publicly available through the CERA WDC Climate database at https://cera-www.dkrz.de/WDCC/ui/cerasearch website. The database can be accessed free of charge after registration. The experiments discussed in the manuscript are available via the following links: FixedSST (https://cera-www.dkrz.de/WDCC/ui/cerasearch/entry?acronym=DKRZ_LTA_519_ds00001), Natural (https://cera-www.dkrz.de/WDCC/ui/cerasearch/entry?acronym=DKRZ_LTA_519_ds00005), NoQBO (https://cera-www.dkrz.de/WDCC/ui/cerasearch/entry?acronym=DKRZ_LTA_519_ds00008), and RCP85 (https://cera-www.dkrz.de/WDCC/ui/cerasearch/entry?acronym=DKRZ_LTA_519_ds00012). All data sets were produced as part of the NATHAN project, which is described in Matthes and Wahl (2015). World Data Center for Climate (WDCC) at DKRZ (http://cera-www.dkrz.de/WDCC/ui/Compact.jsp?acronym=DKRZ_lta_519). We thank the two anonymous reviewers for their helpful comments.

## References

Abalichin, J. (2016). Natürliche Variabilität und anthropogener Einfluss in Simulationen mit gekoppeltem Klima-Chemie-Modell EMAC-O: Atmosphären-Ozean-Wechselwirkungen im Klimawandel der Südhemisphäre. PhD thesis, Freie Universität Berlin. Retrieved from https://refubium.fu-berlin.de/handle/fub188/4313

Ayarzagüena, B., Polvani, L. M., Langematz, U., Akiyoshi, H., Bekki, S., Butchart, N., et al. (2018). No robust evidence of future changes in major stratospheric sudden warmings: A multi-model assessment from CCMI. *Atmospheric Chemistry and Physics*, *18*(15), 11,277–11,287. https://doi.org/10.5194/acp-18-11277-2018

Ayarzagüena, B., & Serrano, E. (2009). Monthly characterization of the tropospheric circulation over the Euro-Atlantic area in relation with the timing of stratospheric final warming. *Journal of Climate*, *22*(23), 6313–6324. https://doi.org/10.1175/2009JCLI2913.1

Bell, C. J., Gray, L. J., & Kettleborough, J. (2010). Changes in the Northern Hemisphere, stratospheric variability under increased $CO_2$ concentrations. *Quarterly Journal of the Royal Meteorological Society*, *136*, 1181–1190.

Black, R. X., & McDaniel, B. A. (2007). The dynamics of Northern Hemisphere stratospheric final warming events. *Journal of the Atmospheric Sciences*, *64*, 2932–2946. https://doi.org/10.1175/JAS3981.1

Black, R. X., McDaniel, B. A., & Robinson, W. A. (2006). Stratosphere-troposphere coupling during spring onset. *Journal of Climate*, *19*(19), 4891–4901. https://doi.org/10.1175/JCLI3907.1

Calvo, N., Giorgetta, M. A., & Peña-Ortiz, C. (2007). Sensitivity of the boreal winter circulation in the middle atmosphere to the quasi-biennial oscillation in MAECHAM5 simulations. *Journal of Geophysical Research*, *112*, D10124. https://doi.org/10.10296/2006JD007844

Calvo, N., Iza, M., Hurwitz, M. M., Manzini, E., Peña-Ortiz, C., Butler, A. H., et al. (2017). Northern Hemisphere stratospheric pathway of different El Niño flavors in stratosphere-resolving CMIP5 models. *Journal of Climate*, *30*, 4351–4371. https://doi.org/10.1175/JCLI-D-16-0132.1

Camp, C. D., & Tung, K. K. (2007). The influence of the solar cycle and QBO on the late winter stratospheric polar vortex. *Journal of the Atmospheric Sciences*, *64*(4), 1267–1283. https://doi.org/10.1175/JAS3883.1

Czaja, A., & Frankignoul, C. (2002). Observed impact of Atlantic SST anomalies on the North Atlantic Oscillation. *Journal of Climate*, *15*(6), 606–623. https://doi.org/10.1175/1520-0442(2002)015<0606:OIOASA>2.0.CO;2

Dee, D. P., Uppala, S. M., Simmons, A. J., Berrisford, P., Poli, P., Kobayashi, S., et al. (2011). The ERA-Interim reanalyses: Configuration and performance of the data assimilation system. *Quarterly Journal of the Royal Meteorological Society*, *137*(656), 553–597. https://doi.org/10.1002/qj.828

Domeisen, D. I., Garfinkel, C. I., & Butler, A. H. (2019). The teleconnection of El Niño Southern Oscillation to the stratosphere. *Reviews of Geophysics*, *57*, 5–47. https://doi.org/10.1029/2018RG000596

Garfinkel, C. I., & Hartmann, D. L. (2008). Different ENSO teleconnections and their effects on the stratospheric polar vortex. *Journal of Geophysical Research*, *113*, D18114. https://doi.org/10.1029/2008JD009920

Gent, P. R., Danabasoglu, G., Donner, L. J., Holland, M. M., Hunke, E. C., Jayne, S. R., et al. (2011). The Community Climate System Model version 4. *Journal of Climate*, *24*(19), 4973–4991. https://doi.org/10.1175/2011JCLI4083.1

Gray, L. J., Crooks, S., Pascoe, C., Sparrow, S., & Palmer, M. (2004). Solar and QBO influences on the timing of stratospheric sudden warmings. *Journal of the Atmospheric Sciences*, *61*(23), 2777–2796. https://doi.org/10.1175/JAS-3297.1

Gray, L. J., Phipps, S. J., Dunkerton, T. J., Baldwin, M. P., Drysdale, E. F., & Allen, M. R. (2001). A data study of the influence of the equatorial upper stratosphere on Northern Hemisphere stratospheric sudden warmings. *Quarterly Journal of the Royal Meteorological Society*, *127*(576), 1985–2003. https://doi.org/10.1002/qj.49712757607

Hansen, F., Matthes, K., & Gray, L. J. (2013). Sensitivity of stratospheric dynamics and chemistry to QBO nudging width in the chemistry-climate model WACCM. *Journal of Geophysical Research: Atmospheres*, *118*, 10,464–10,474. https://doi.org/10.1002/jgrd.50812

Hansen, F., Matthes, K., Petrick, C., & Wang, W. (2014). The influence of natural and anthropogenic factors on major stratospheric sudden warmings. *Journal of Geophysical Research: Atmospheres*, *119*, 8117–8136. https://doi.org/10.1002/2013JD021397

Hardiman, S. C., Butchart, N., Charlton-Perez, A. J., Shaw, T. A., Akiyoshi, H., Baumgaertner, A., et al. (2011). Improved predictability of the troposphere using stratospheric final warmings. *Journal of Geophysical Research*, *116*, D18113. https://doi.org/10.1029/2011JD015914

Holton, J. R., & Tan, H.-C. (1980). The influence of the equatorial quasi-biennial oscillation on the global circulation at 50 mb. *Journal of the Atmospheric Sciences*, *37*(10), 2200–2208. https://doi.org/10.1175/1520-0469(1980)037<2200:TIOTEQ>2.0.CO;2

Hu, J., Ren, R., & Xu, H. (2014). Occurrence of winter stratospheric sudden warming events and the seasonal timing of spring stratospheric final warming. *Journal of the Atmospheric Sciences*, *71*(7), 2319–2334. https://doi.org/10.1175/JAS-D-13-0349.1

Hurwitz, M. M., Newman, P. A., & Garfinkel, C. I. (2012). On the influence of North Pacific sea surface temperature on the Arctic winter climate. *Journal of Geophysical Research*, *117*, D19110. https://doi.org/10.1029/2012JD017819

Ivy, D. J., Solomon, S., & Thompson, D. W. (2014). On the identification of the downward propagation of Arctic stratospheric climate change over recent decades. *Journal of Climate*, *27*(8), 2789–2799. https://doi.org/10.1175/JCLI-D-13-00445.1

Jöckel, P., Tost, H., Pozzer, A., Brühl, C., Buchholz, J., Ganzeveld, L., et al. (2006). The atmospheric chemistry general circulation model ECHAM5/MESSy: Consistent simulation of ozone from the surface to the mesosphere. *Atmospheric Chemistry and Physics*, *6*(12), 5067–5104. https://doi.org/10.5194/acp-6-5067-2006

Jungclaus, J. H., Keenlyside, N., Botzet, M., Haak, H., Luo, J. J., Latif, M., et al. (2006). Ocean circulation and tropical variability in the coupled model ECHAM5/MPI-OM. *Journal of Climate*, *19*(16), 3952–3972. https://doi.org/10.1175/JCLI3827.1

Karpechko, A. Y., & Manzini, E. (2017). Arctic stratosphere dynamical response to global warming. *Journal of Climate*, *30*(17), 7071–7086. https://doi.org/10.1175/JCLI-D-16-0781.1

Kim, J., Son, S.-W., Gerber, E. P., & Park, H.-S. (2017). Defining sudden stratospheric warming in climate models: Accounting for biases in model climatologies. *Journal of Climate*, *30*(14), 5529–5546. https://doi.org/10.1175/JCLI-D-16-0465.1

Kinnison, D. E., Brasseur, G. P., Walters, S., Garcia, R. R., Marsh, D. R., Sassi, F., et al. (2007). Sensitivity of chemical tracers to meteorological parameters in the MOZART-3 chemical transport model. *Journal of Geophysical Research*, *112*, D20302. https://doi.org/10.1029/2006JD007879

Kuttippurath, J., & Nikulin, G. (2012). A comparative study of the major sudden stratospheric warmings in the Arctic winters 2003/2004–2009/2010. *Atmospheric Chemistry and Physics*, *12*(17), 8115–8129. https://doi.org/10.5194/acp-12-8115-2012

Labitzke, K. (1981). Stratospheric-mesospheric midwinter disturbances: A summary of observed characteristics. *Journal of Geophysical Research*, *86*(C10), 9665–9678. https://doi.org/10.1029/JC086iC10p09665

Lean, J. L., Rottman, G., Harder, J., & Kopp, G. (2005). Source contributions to new understanding of global change and solar variability. *Solar Physics*, *230*, 27–53. https://doi.org/10.1007/s11207-005-1527-2

Lubis, S. W., Matthes, K., Omrani, N., Harnik, N., & Wahl, S. (2016). Influence of the quasi-biennial oscillation and sea surface temperature variability on downward wave coupling in the Northern Hemisphere. *Journal of the Atmospheric Sciences*, *73*(5), 1943–1965. https://doi.org/10.1175/JAS-D-15-0072.1

Lubis, S. W., Omrani, N., Matthes, K., & Wahl, S. (2016). Impact of the Antarctic ozone hole on the vertical coupling of the stratosphere-mesosphere-lower thermosphere system. *Journal of the Atmospheric Sciences*, *73*, 2509–2528. https://doi.org/10.1175/JAS-D-15-0189.1

Manney, G. L., & Lawrence, Z. D. (2016). The major stratospheric final warming in 2016: dispersal of vortex air and termination of Arctic chemical ozone loss. *Atmospheric Chemistry and Physics*, *16*, 15,371–15,396. https://doi.org/10.5194/acp-16-15371-2016

Manney, G. L., Livesey, N. J., Jimenez, C. J., Pumphrey, H. C., Santee, M. L., MacKenzie, I. A., & Waters, J. W. (2006). EOS Microwave Limb Sounder observations of "frozen-in" anticyclonic air in Arctic summer. *Geophysical Research Letters*, *33*, L06810. https://doi.org/10.1029/2005GL025418

Manney, G. L., Santee, M. L., Froidevaux, L., Hoppel, K., Livesey, N. J., & Waters, J. W. (2006). EOS MLS observations of ozone loss in the 2004-2005 Arctic winter. *Geophysical Research Letters*, *33*, L04802. https://doi.org/10.1029/2005GL024494

Manney, G. L., Santee, M. L., Rex, M., Livesey, N. J., Pitts, M. C., Veefkind, P., et al. (2011). Unprecedented Arctic ozone loss in 2011. *Nature*, *478*(7370), 469–475. https://doi.org/10.1038/nature10556

Manzini, E., Karpechko, A. Y., Anstey, J., Baldwin, M. P., Black, R. X., Cagnazzo, C., et al. (2014). Northern winter climate change: Assessment of uncertainty in CMIP5 projections related to stratosphere-troposphere coupling. *Journal of Geophysical Research: Atmospheres*, *119*, 7979–7998. https://doi.org/10.1002/2013JD021403

Marsh, D., Mills, M. J., Kinnison, D. E., Lamarque, J.-F., Calvo, N., & Polvani, L. M. (2013). Climate change from 1850 to 2005 simulated in CESM1(WACCM). *Journal of Climate*, *26*(19), 7372–7391. https://doi.org/10.1175/JCLI-D-12-00558.1

Matthes, K., Kodera, K., Garcia, R. R., Kuroda, Y., Marsh, D. R., & Labitzke, K. (2013). The importance of time-varying forcing for QBO modulation of the atmospheric 11 year solar cycle signal. *Journal of Geophysical Research: Atmospheres*, *118*, 4435–4447. https://doi.org/10.1002/jgrd.50424

Matthes, K., Marsh, D. R., Garcia, R. R., Kinnison, D. E., Sassi, F., & Walters, S. (2010). Role of the QBO in modulating the influence of the 11 year solar cycle on the atmosphere using constant forcings. *Journal of Geophysical Research*, *115*, D18110. https://doi.org/10.1029/2009JD013020

Matthes, K., & Wahl, S. (2015). NATHAN-Quantification of Natural Climate Variability in the Atmosphere-Hydrosphere System with Data Constrained Simulations. World Data Center for Climate (WDCC) at DKRZ. Retrieved from http://cera-www.dkrz.de/WDCC/ui/Compact.jsp?acronym=DKRZ_lta_519

Meinshausen, M., Smith, S. J., Calvin, K., Daniel, J. S., Kainuma, M. L. T., Lamarque, J. F., et al. (2011). The RCP greenhouse gas concentrations and their extensions from 1765 to 2300. *Climatic Change*, *109*(1–2), 213–241. https://doi.org/10.1007/s10584-011-0156-z

Mitchell, D. M., Osprey, S., Gray, L. J., Butchart, N., Hardiman, S. C., Charlton-Perez, A. J., & Watson, P. (2012). The effect of climate change on the variability of the Northern Hemisphere stratospheric polar vortex. *Journal of the Atmospheric Sciences*, *69*(8), 2608–2618. https://doi.org/10.1175/JAS-D-12-021.1

Mlynczak, M. G., Mertens, C. J., Garcia, R. R., & Portmann, R. W. (1999). A detailed evaluation of the stratospheric heat budget: 2. Global radiation balance and diabatic circulations. *Journal of Geophysical Research*, *104*, 6039–6066. https://doi.org/10.1029/1998JD200099

Mudelsee, M. (2014). *Climate Time Series Analysis: Classical Statistical and Bootstrap Methods* (2nd ed., Vol. 717). Cham Heidelberg New York Dordrecht London: Springer.

Naujokat, B. (1986). An update of the observed quasi-biennial oscillation of the stratospheric winds over the tropics. *Journal of the Atmospheric Sciences*, *43*(17), 1873–1877. https://doi.org/10.1175/1520-0469(1986)043<1873:AUOTOQ>2.0.CO;2

Omrani, N.-E., Keenlyside, N., Bader, J., & Manzini, E. (2014). Stratosphere key for wintertime atmospheric response to warm Atlantic decadal conditions. *Climate Dynamics*, *42*(3-4), 649–663. https://doi.org/10.1007/s00382-013-1860-3

Previdi, M., & Polvani, L. M. (2014). Climate system response to stratospheric ozone depletion and recovery. *Quarterly Journal of the Royal Meteorological Society*, *140*(685), 2401–2419. https://doi.org/10.1002/qj.2330

Salby, M. L., & Callaghan, P. F. (2007). Influence of planetary wave activity on the stratospheric final warming and spring ozone. *Journal of Geophysical Research*, *112*, D20111. https://doi.org/10.1029/2006JD00753

SPARC CCMVal. (2010). SPARC report on the evaluation of Chemistry-Climate Models, V. Eyring, T. G. Shepherd, D. W. Waugh (Eds.), SPARC Report No. 5, WCRP-132, WMO/TD-No. 1526.

Thiéblemont, R., Huret, N., Orsolini, Y. J., Hauchecorne, A., & Drouin, M.-A. (2011). Frozen-in anticyclones occurrinsg in polar Northern Hemisphere during springtime: Characterization, occurrence and link with quasi-biennial oscillation. *Journal of Geophysical Research*, *116*, D20110. https://doi.org/10.1029/2011JD016042

Thiéblemont, R., Orsolini, Y. J., Hauchecorne, A., Drouin, M.-A., & Huret, N. (2013). A climatology of frozen-in anticyclones in the spring arctic stratosphere over the period 1960–2011. *Journal of Geophysical Research: Atmospheres*, *118*, 1299–1311. https://doi.org/10.1002/jgrd.50156

Visbeck, M., Chassignet, E., Curry, R., Delworth, T., Dickson, B., & Krahmann, G. (2003). The ocean's response to North Atlantic oscillation variability. In J. Hurrell, Y. Kushnir, G. Ottersen, & M. Visbeck (Eds.), *The North Atlantic Oscillation*, *Geophysical Monograph Series* (pp. 1–36). Washington, DC: American Geophysical Union.

Waugh, D. W., Randel, W. J., Pawson, S., Newman, P. A., & Nash, E. R. (1999). Persistence of the Lower Stratospheric Polar Vortices. *Journal of Geophysical Research*, *104*(D22), 27,191–27,201. https://doi.org/10.1029/1999JD900795

Waugh, D. W., & Rong, P. P. (2002). Interannual variability in the decay of lower stratospheric Arctic vortices. *Journal of the Meteorological Society of Japan*, *80*(4B), 997–1012. https://doi.org/10.2151/jmsj.80.997

Wei, K., Chen, W., & Huang, R. H. (2007). Dynamical diagnosis of the breakup of the stratospheric polar vortex in the Northern Hemisphere. *Science in China Series D-Earth Sciences*, *50*(9), 1369–1379. https://doi.org/10.1007/s11430-007-0100-2